# Analysis of ionospheric anomalies before earthquakes with Mw6.5 and above in Japan during 2011-2022

**Zhen Li**
North China University of Water Resources and Electric Power
**Zhen Tao**
North China University of Water Resources and Electric Power
**Lianhai Cao**
caolianhai@ncwu.edu.cn

North China University of Water Resources and Electric Power

**Article**

**Keywords:** wavelet power spectrum, Ionospheric disturbance, LAIC, The Japanese earthquake, Time series

**Posted Date:** February 22nd, 2024

**DOI:** https://doi.org/10.21203/rs.3.rs-3939095/v1



**Additional Declarations:** No competing interests reported.

# Analysis of ionospheric anomalies before earthquakes with Mw6.5 and above in Japan during 2011-2022

Zhen Li[1,2], Zhen Tao[1], Lianhai Cao[*1]

[1]College of Surveying and Geo-Informatics, North China University of Water Resources and Electric Power, 136 East Jinshui Road, Zhengzhou, 450046, Henan, China.
[2]State Key Laboratory, Geo-information Engineering, Street, Xi'an, 710054, Shanxi, China.
Correspondence: Lianhai Cao, caolianhai@ncwu.edu.cn
Author email: Zhen Li email: lizhenhhu@126.com
Zhen Tao email: taozhen753@163.com

**Abstract:** In order to study the seismic-ionospheric coupling relationship, this paper selects window values based on wavelet power spectrum method, and obtains the 27-day periodicity of wavelet power spectrum in the full time domain that passes 95% significance test. Then, sliding quartile method is used to analyze the earthquakes above Mw6.5 in Japan from 2011 to 2022, which exclude hybrid effects. Sunspot number (SSN), 10.7cm radio flux (F10.7), solar wind velocity (Vsw), storm ring current index (DST), and global Geomagnetic activity index (KP) are excluded as interference terms to eliminate the influence of solar and geomagnetic activity. According to the lithosphere-atmosphere-ionospheric coupling mechanism (LAIC) and global TECmap, the abnormal changes on the 29th day before the earthquake (February 15, 2022), which do not conform to the previous research rules, are analyzed to prove that TEC anomalies caused by earthquakes. The statistical analysis of ionospheric TEC anomalies shows that the magnitude of earthquake is positively correlated with the amplitude of TEC anomalies, and the occurrence time of ionospheric anomalies tends to lag as the magnitude increases.

**Key words:** wavelet power spectrum; Ionospheric disturbance; LAIC; The Japanese earthquake; Time series.

## 1. Introduction

Earthquake has always been one of the most serious natural disasters in nature. Apart from the serious consequences brought by earthquake itself, tsunami and volcanic eruption caused by earthquake chain reaction have brought great threats to human life and property safety. Therefore, how to forewarn the occurrence of earthquake has always been the focus of many scientists and researchers. As early as the 1960s, Davies and Baker observed the phenomenon of ionospheric effect before and after the Alaska earthquake [1], and verified that the anomalies in the ionosphere may be related to the earthquake, and more and more studies proved

that there were abnormal disturbances in the ionosphere before the earthquake [2-5]. In addition, most of the ionospheric disturbance phenomena existed in the first 15 days after the earthquake [6-7]. Many data show that the seismic process is not only limited to the Earth's lithosphere, destroying and affecting the surface morphology, but also reacts to the atmosphere, ionosphere and magnetosphere through the action of electromagnetic fields, thereby disturbing the ionosphere above and affecting the abnormal change of total electron content (TEC). For a long time, many researchers have attached great importance to the study of the seismo-ionosphere physical mechanism, and put forward many theories based on the different objects studied. Pulinets and Ouzounov proposed the lithosphere-atmosphere-ionospheric coupling (LAIC) model [8], which is mainly reflected in the fact that radon-dominated gas escapes from rock layers during earthquake gestation period, leading to an increase in concentration, which excites the ionosphere to form ion clusters and then changes the electrical conductivity in the air, leading to abnormal changes in TEC. Freund et al proposed a positive hole model during earthquake pregnancy [9-11]. By analyzing the Mw9.0 earthquake in Japan and Mw8.1 earthquake in Nepal in 2011, Quzounov et al. concluded that the ionospheric anomalies were caused by the ionospheric anomalies in response to the outward wave radiation [12-13]. Pulinets et al. believed that the atmospheric ionization process was due to the coupling relationship between the vertical atmospheric electric field and the ionosphere [14-15]. Parrot et al. verified the coupling relationship between atmosphere and ionosphere based on global ionospheric map (GIM), thermal infrared (TIR) anomaly and outgoing long-wave radiation (OLR) data of total electron content (TEC) [16]. Both solar and geomagnetic activities will affect the variation of TEC, and TEC itself also has certain seasonal variation characteristics [17-18]. In addition, many studies have detected the magnetic conjugation effect caused by the seismic-ionospheric coupling before the earthquake [19-21]. In this paper, the GIM TEC data and the seismic-ionospheric coupling mechanism of Mw6.5 + earthquakes in Japan from 2011 to 2022 are studied.

## 2. Data and methodology

### 2.1 Data Acquisition

In this paper, this area of Japan is selected as the object to explore the seismic-ionospheric coupling mechanism. In order to exclude the confusions between different earthquakes occurring in nearby areas [23], no strong earthquakes occurred in the area near the epicentre of the earthquakes with MMW6.5 or above that occurred from 2011 to 2022. This article selects IGS stations obtain the TEC data as the basis of describing the ionosphere state data, the data by the European centre for orbit determination (CODG) around the world about 300 IGS stations real-time monitoring (https://www.aiub.unibe.ch/download). TEC data is modeled by vertical total electron content (VTEC) using spherical harmonic expansion. Since 2014, CODG has reconstructed TEC data with higher 15-order spherical harmonics, and its spatial resolution is 2.5° in dimension and 5° in longitude. After the update, the time resolution of the data has also changed from

2 hours to 1 hour. This makes the global TEC data more accurate and sufficient to satisfy the study of the spatiotemporal variation of the ionosphere as the basic data. However, the data of these grid points are not necessarily located in the vertical sky of the epicenter [24], so this paper uses the nearest grid points around the epicenter for interpolation to calculate the TEC value of the vertical sky. In order to eliminate the factors affecting the ionospheric disturbance, this paper uses the sunspot number (SSN), 10.7cm solar radio flux (F10.7), solar wind velocity (Vsw), global geomagnetic activity index (KP), and magnetic storm ring current index (DST) to analyze and eliminate them by sliding interquart method. The data provided by NASA (NASA) (https://omniweb.gsfc.nasa.gov/form/dx1.html). Sunspot number (SSN) has been observed for more than 300 years and is the main parameter to express solar activity. Solar radio flux (F10.7) The 100 MHz bandwidth centered on 2800 MHz (10.7 cm wavelength) at the center of an hour is an important parameter to determine the intensity of solar radio emission, which is expressed in solar luminous flux units (sfu), usually 50-300 SFU. The DST index is observed once every hour, and -30 ~ 50nt is a weak magnetic burst, 50nT ~ 100nT is a medium magnetic storm, and more than 100nT is divided into large, very large, and very large magnetic storms according to the size of the index. KP index has a temporal resolution of 3h, and KP index is currently divided into 10 levels (KP=0-9)[25]. In this paper, 20 earthquakes are classified according to their magnitude to investigate the relationship between the ionosphere and earthquakes. Figure 1 shows the geographic distribution of the 20 earthquakes that occurred within the area of Japan. Table 1 below provides information about the 20 earthquakes:

Table 1: Information of Mw≥6.5 earthquakes in Japan from December to 2022

| Time of earthquake occurrence | | | | | | Earthquake location | | | |
|---|---|---|---|---|---|---|---|---|---|
| No. | Year | Month | Day | Hour | Minute | Latitude | Longitude | Hypocenter Depth/km | Mw |
| 1 | 2014 | 07 | 11 | 19 | 22 | 37.01 | 142.45 | 20 | 6.5 |
| 2 | 2011 | 03 | 11 | 08 | 19 | 36.17 | 141.56 | 7 | 6.5 |
| 3 | 2018 | 09 | 05 | 18 | 08 | 42.69 | 141.93 | 35 | 6.6 |
| 4 | 2011 | 04 | 11 | 08 | 16 | 37.00 | 140.40 | 11 | 6.6 |
| 5 | 2015 | 02 | 16 | 23 | 06 | 39.86 | 142.88 | 23 | 6.7 |
| 6 | 2016 | 01 | 14 | 03 | 25 | 41.97 | 142.78 | 46 | 6.7 |
| 7 | 2011 | 09 | 16 | 19 | 26 | 40.27 | 142.78 | 30 | 6.7 |
| 8 | 2012 | 01 | 01 | 05 | 27 | 31.46 | 138.07 | 365 | 6.8 |
| 9 | 2015 | 05 | 12 | 21 | 12 | 38.91 | 142.03 | 35 | 6.8 |
| 10 | 2012 | 03 | 14 | 09 | 08 | 40.89 | 144.94 | 12 | 6.9 |
| 11 | 2013 | 02 | 02 | 14 | 17 | 42.77 | 143.09 | 107 | 6.9 |
| 12 | 2016 | 11 | 21 | 20 | 59 | 37.39 | 141.39 | 9 | 6.9 |
| 13 | 2021 | 05 | 01 | 0 | 27 | 38.20 | 141.60 | 43 | 6.9 |

| | | | | | | | | | |
|---|---|---|---|---|---|---|---|---|---|
| 14 | 2016 | 04 | 15 | 16 | 25 | 32.79 | 130.75 | 10 | 7 |
| 15 | 2021 | 03 | 20 | 09 | 09 | 38.45 | 141.65 | 43 | 7 |
| 16 | 2011 | 07 | 10 | 07 | 57 | 38.03 | 143.26 | 23 | 7 |
| 17 | 2013 | 10 | 25 | 17 | 10 | 37.16 | 144.66 | 35 | 7.1 |
| 18 | 2021 | 02 | 13 | 14 | 07 | 37.73 | 141.78 | 44 | 7.1 |
| 19 | 2012 | 12 | 07 | 08 | 18 | 37.89 | 143.95 | 31 | 7.3 |
| 20 | 2022 | 03 | 16 | 14 | 36 | 37.71 | 141.58 | 41 | 7.3 |

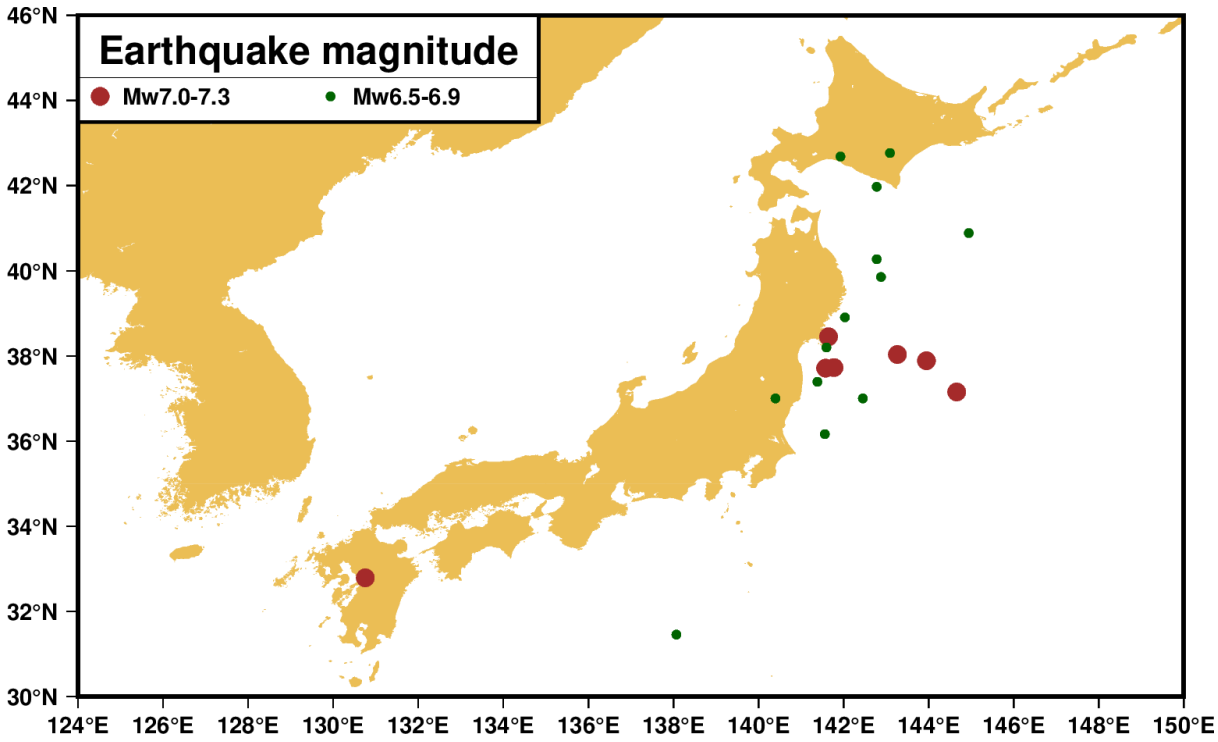


Figure 1 Geographical distribution of 20 earthquakes in Japan during 2011-2022; The red dot represents the epicenter of the Mw7.0-7.3 earthquake, and the green dot represents the epicenter of the Mw6.5-6.9 earthquake

## 2.2 Methods

### 2.2.1 Wavelet analysis

As the solar rotation has a periodicity of 27 days, the solar radiation also has a periodicity of 27 days [26]. The ultraviolet rays, X-rays and solar wind caused by it all act on the atmosphere, and the ionosphere is also affected by it. In order to quantitatively analyze this influence on the cycle, the periodic influence of the ionosphere can be excluded. In this paper, the method of wavelet analysis is used to explore the periodic window. Wavelet analysis is an analysis method used to analyze the power spectrum of time series. Compared with Fourier transform, it can eliminate the influence of edge effect on the period. In the selection of parent wavelet, this paper chooses Morlet wavelet, which has better localization property in frequency domain and time domain [27].

The specific expression of Morlet wavelet is:

$$\psi(t) = e^{-at^2}\cos(5t) \quad (1)$$

Where, is the scaling factor, the wavelet transform of the signal is defined as:

$$w_f(a,b) = \int_R f(t)\overline{\psi}_{ab}(t)dt \quad (2)$$

where $\overline{\psi}_{ab}(t)$ is the conjugate function of $\psi_{ab}(t)$, $b$ is the translation factor.

The wavelet power spectrum is defined as:

| | | |
|---|---|---|
| | $E_{a,b} = \left\|W_f(a,b)\right\|^2$ | (3) |

The global wavelet power spectrum is used to represent the energy density corresponding to different scales:

| | | |
|---|---|---|
| | $E_a = \frac{1}{N}\sum_{b}^{N}\left\|W_f(a,b)\right\|^2$ | (4) |

The period of TEC in the local time domain was obtained using the wavelet power spectrum, and the period was tested with 95% significance. The period that passed the test was taken as the window value and the influence of solar and geomagnetic activities on the ionosphere was excluded based on the sliding quartile method.The main principle of sliding quartile distance method is to select the values of TEC at the same time every day and sort them in ascending order, and then divide the sequence into four parts, including lower quartile Q1, middle quartile Q2 and upper quartile Q3.

| | | |
|---|---|---|
| | $Q_1 = \frac{(x_7 + x_8)}{2}$ | (5) |
| | $Q_2 = \frac{(x_{14} + x_{15})}{2}$ | (6) |
| | $Q_3 = \frac{(x_{21} + x_{22})}{2}$ | (7) |

Where the interquartile distance can be calculated as:

| | | |
|---|---|---|
| | $IQR = Q_3 - Q_1$ | (8) |

IQR is approximately equal to 1.349 times the standard deviation, and 1.5IQR is approximately equal to 2 times the standard deviation (distribution probability is 95.44%) to satisfy the 95% confidence interval. Therefore, this paper uses 1.5IQR as the standard value l1 and l2 as the upper and lower limits of the anomaly test, respectively

| | | |
|---|---|---|
| | $l_1 = Q_2 + 1.5IQR$ | (9) |
| | $l_2 = Q_2 - 1.5IQR$ | (10) |

TEC values beyond the upper and lower limits are considered outliers:

| | | |
|---|---|---|
| | $\Delta TEC = \begin{cases} TEC - l_1; & while TEC > l_1 \\ 0; & while TEC < l_1, TEC > l_2 \\ TEC - l_2; & while TEC < l_2 \end{cases}$ | (11) |

## 3. Results

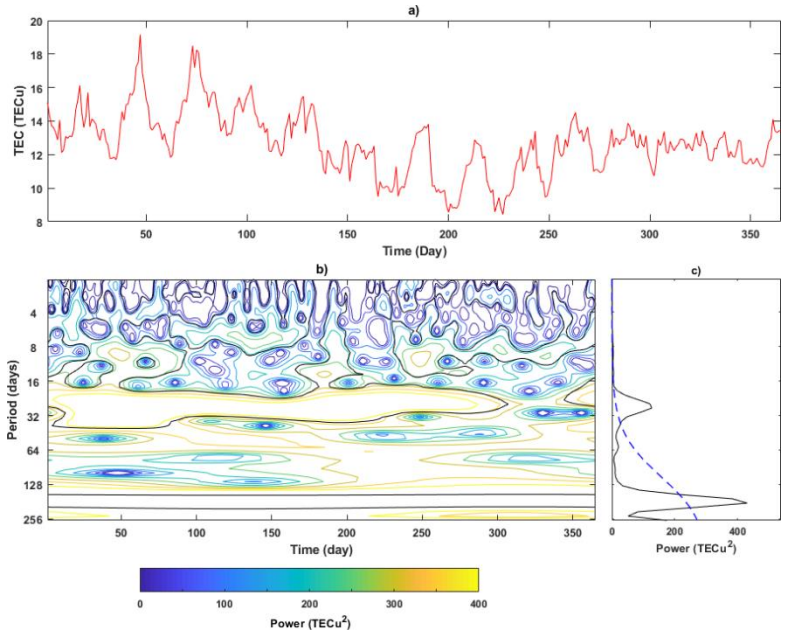


Figure 2. TEC periodic spectrum analysis in 2005 (a)TEC time series (b)TEC Morlet wavelet analysis power spectrum (c)TEC overall periodic spectrum

In this paper, the average daily TEC value in 2005 is used to verify its period by wavelet analysis. It can be seen from Figure 2(b) that TEC has significant periods in the 16-32-day period and the 128-256 day period, among which the 16-32-day period exists in most time domains, while the 128-256 day period is significant in all time domains. It can be seen from Figure 2(c) that the periods of 27.8 days and 187 days in the overall periodic spectrum pass the 95% significance test, indicating that these two periods are significant in the global time domain, proving that the ionosphere also has a periodicity of 27 days due to solar activities. Therefore, in this paper, data from 30 days before each earthquake to 2 days after each earthquake are processed according to the sliding quartile distance method with 27 days as the window value. Figure 3-7 shows the solar and geomagnetic activity data after processing, and Figure 9 shows the TEC data after processing.

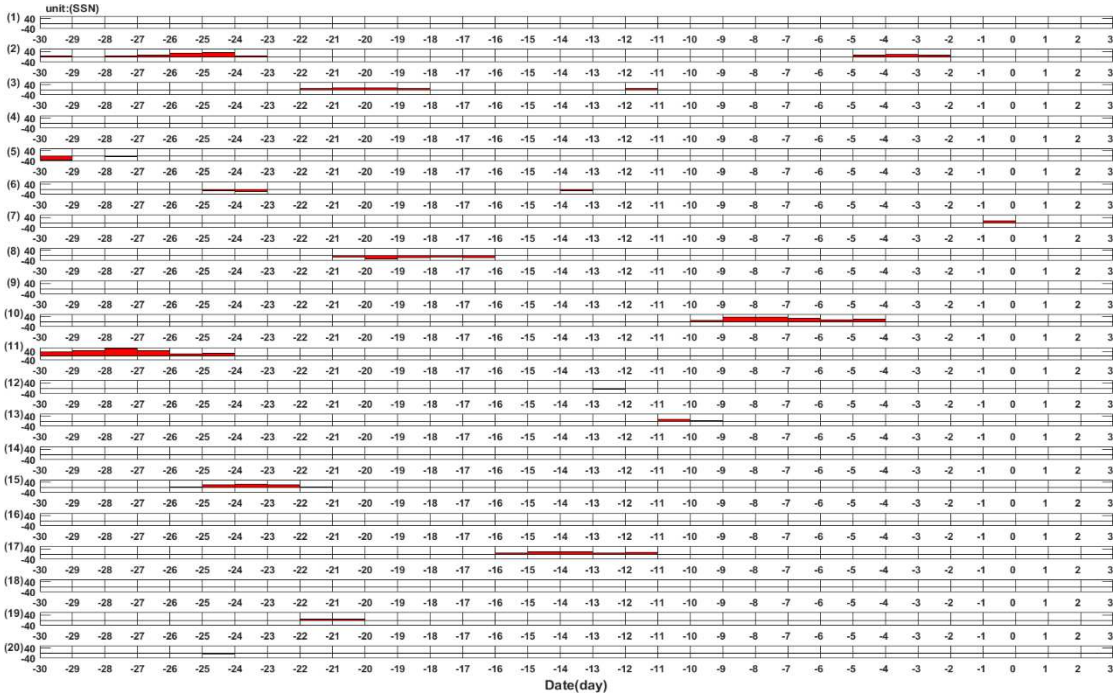


Figure 3 Changes of sunspots (SSNS) during Japan Mw6.5 + earthquake from 2011 to 2022

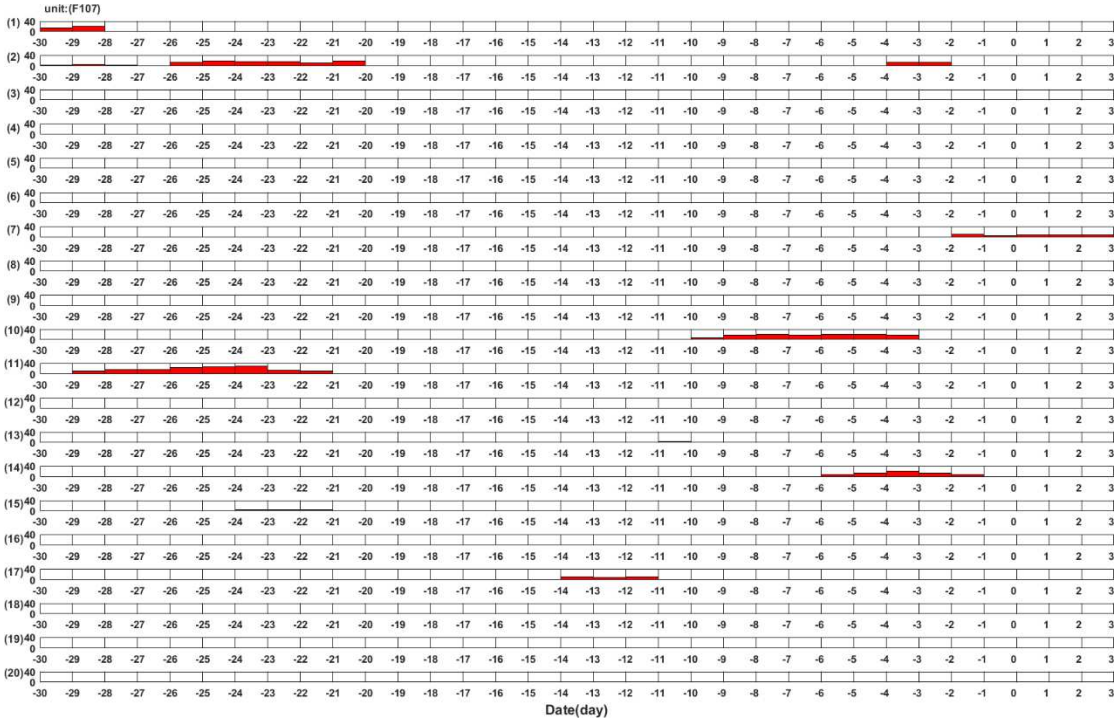


Figure 4 Changes of 10.7cm radio flux (F10.7) in Japan Mw6.5 earthquakes during 2011-2022

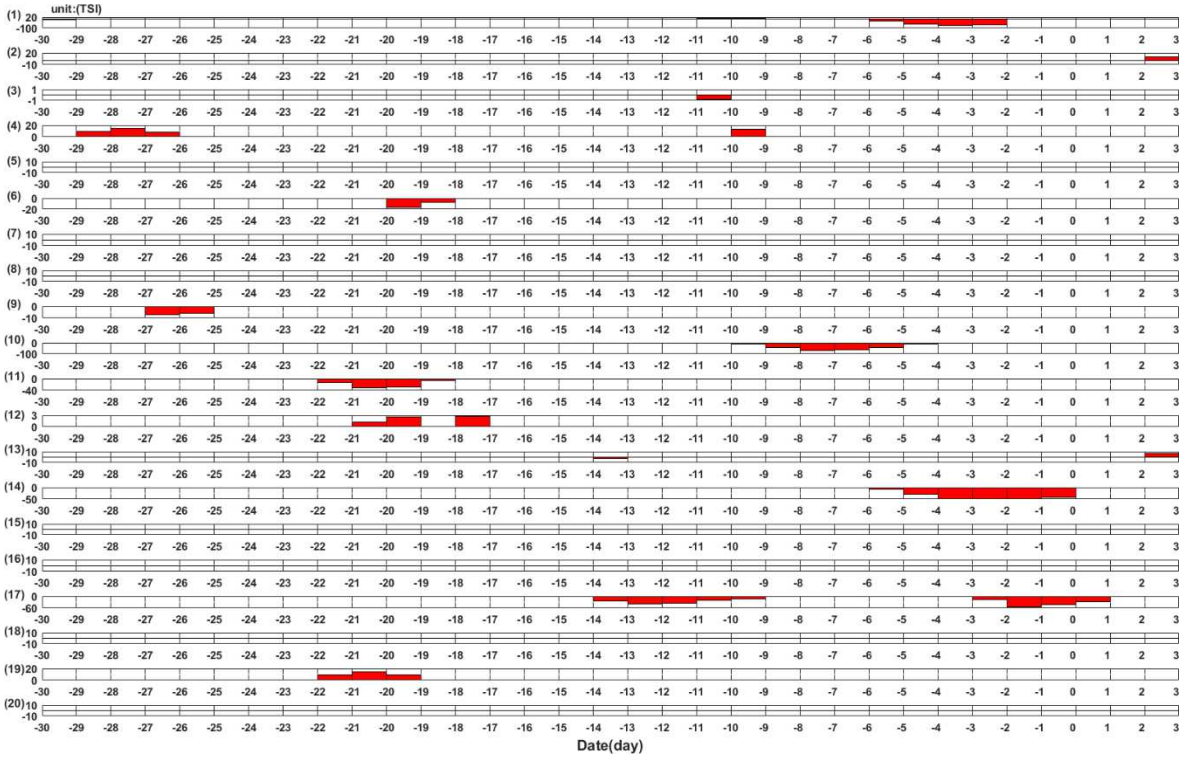


Figure 5 Change of total solar radiation (TSI) for earthquakes with MMW6.5 or above in Japan from 2011 to 2022

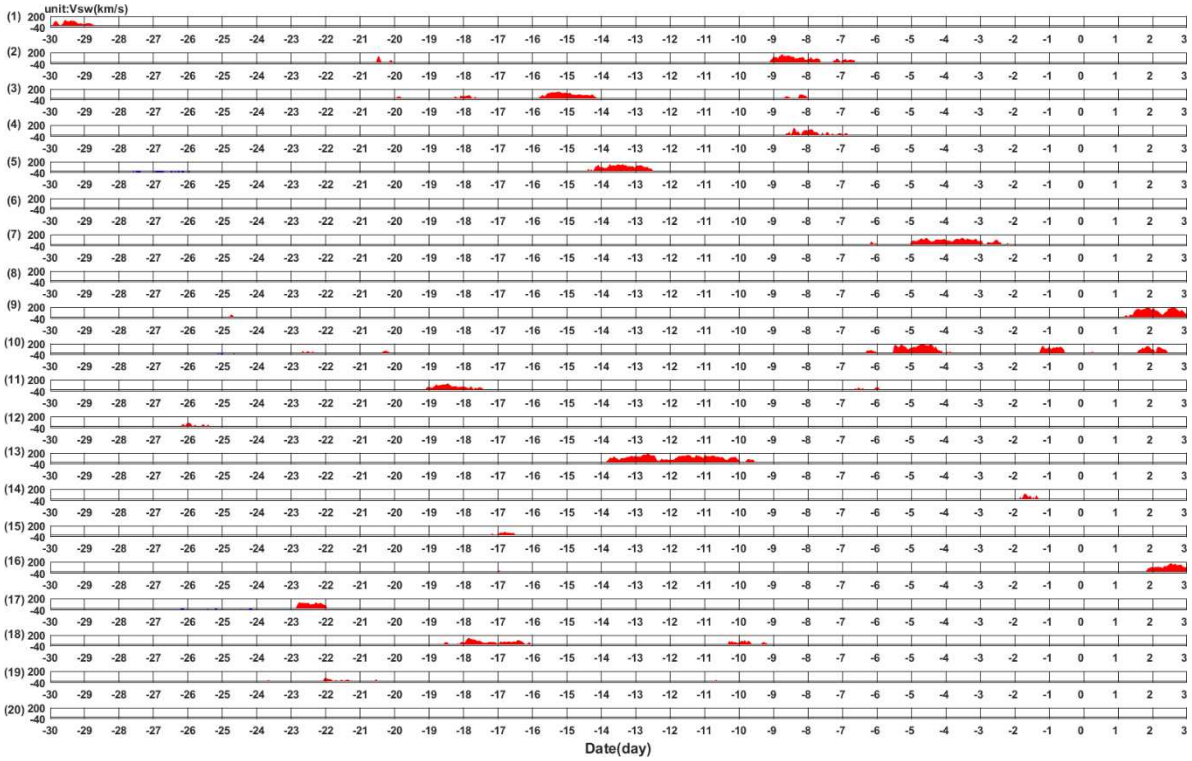


Figure 6 Variation of solar wind velocity (Vsw) for earthquakes above MMW6.5 in Japan during 2011-2022

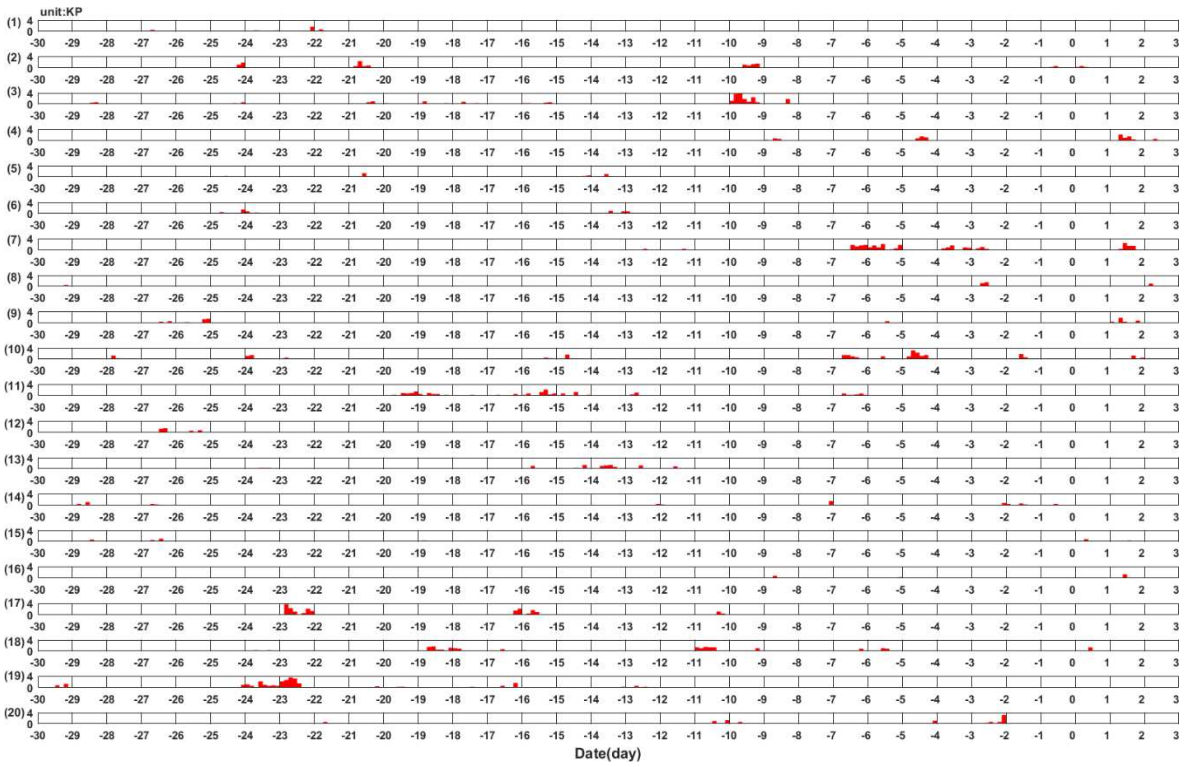


Figure 7 Changes of the Global Geomagnetic Activity Index (KP) of the Japan Mw6.5 + earthquakes from 2011 to 2022

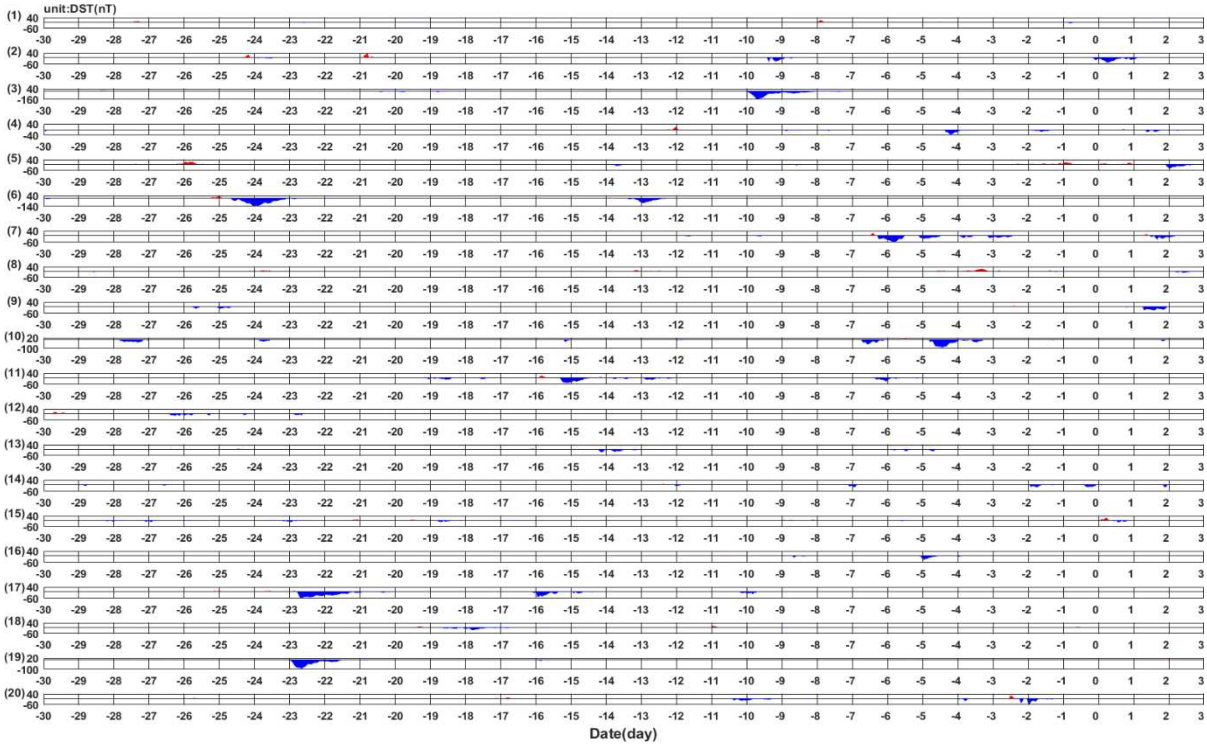


Figure 8. The change of ring current index (DST) of seismic magnetic storms above MMW6.5 in Japan from 2011 to 2022

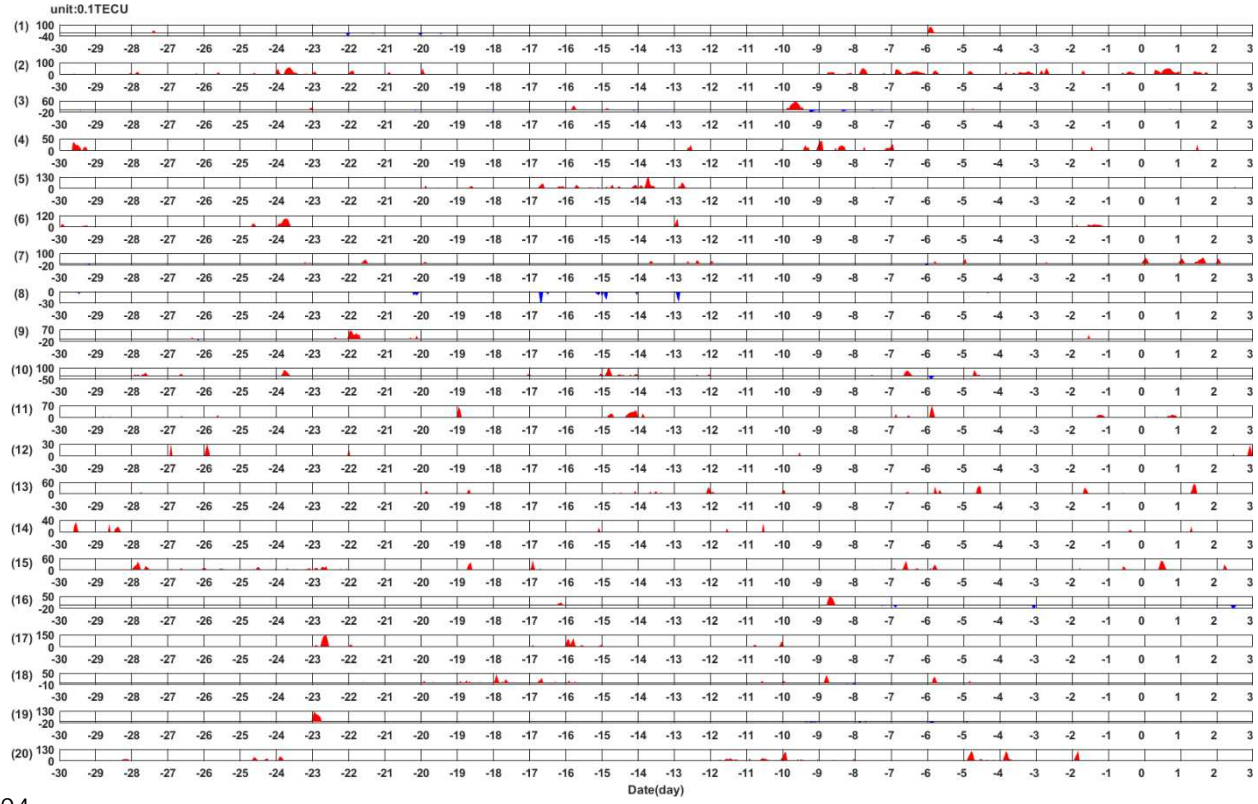


Figure 9. TEC changes in Japan Mw6.5 + earthquakes from 2011 to 2022

It can be seen from FIG. 3-6 that in the 20 selected earthquakes, solar activity varied to different degrees from 30 days before the earthquake to 2 days after the earthquake, but the number of abnormal changes was less than that of geomagnetic activity. It can be seen from FIG. 7-8 that the occurrence of geomagnetic activity anomalies is more frequent and the distribution is more dispersed, and the amplitude of some abnormal changes is larger, which may indicate the occurrence of large or medium-sized magnetic storms. It can be seen from Figure 9 that in addition to the abnormal TEC disturbance in the 15 days studied before, there was also abnormal TEC disturbance 15 days before, which may be caused by solar and geomagnetic activities. Therefore, in order to eliminate the interference of solar activity and geomagnetic activity on the ionosphere, the time period of TEC anomaly and the same time period of solar activity and geomagnetic activity data anomaly are eliminated. The red and blue areas above and below the zero line represent positive and negative TEC anomalies, respectively. After analysis and statistics, 65%(13 out of 20 earthquakes) of Mw6.5 or more earthquakes occurred before the TEC anomaly, and several TEC anomalies were found before some earthquakes, such as the 12 earthquake two days after the earthquake, 10 days before the earthquake, 13 earthquake 1 day after the earthquake, 2 days before the earthquake. No TEC anomalies were found in earthquakes 1, 3, 8, 10, 17, 18 and 19 after excluding solar and geomagnetic activities. TEC anomalies were also found 15 days before individual earthquakes, but all of them were minor anomalies, and all of them were global disturbances observed by VTECmap, and did not have the characteristics of ionospheric

anomalies caused by earthquakes. But we found an ionospheric anomaly 29 days before the 20th earthquake, a special phenomenon described in more detail below.

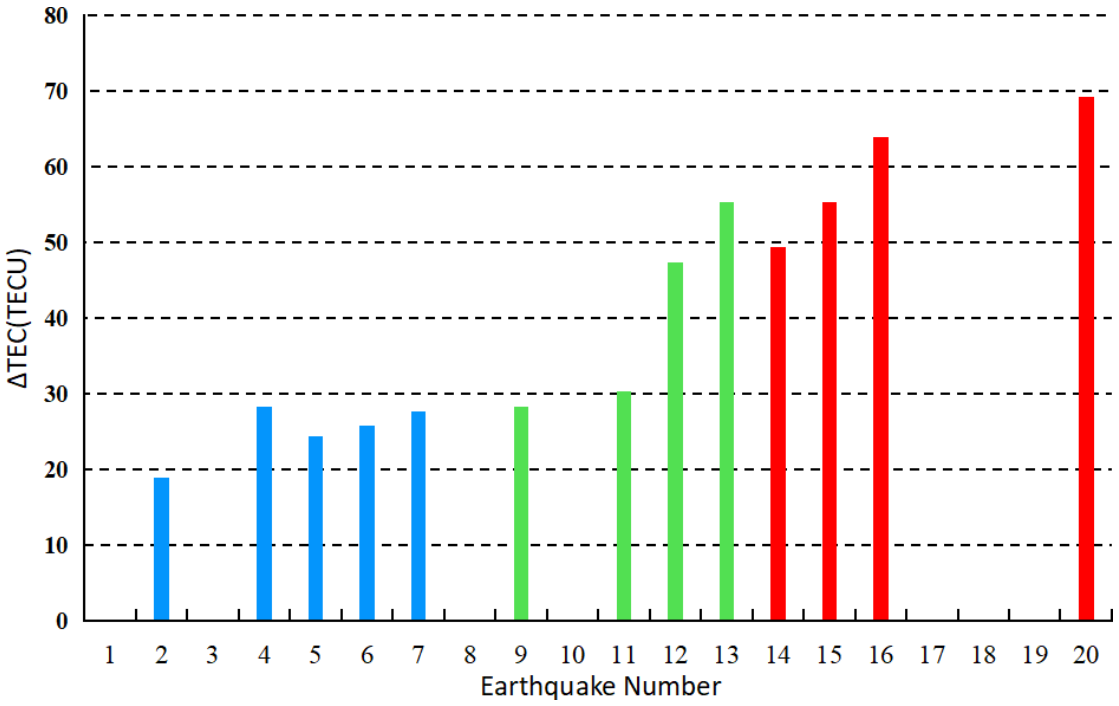


Figure 10. TEC anomaly amplitude at the epicenter before the earthquake

Considering that the ionospheric anomaly occurs more than once, we choose the maximum amplitude of the anomaly to represent the TEC anomaly of the relevant earthquake. Figure 10 shows the maximum amplitude of the ionospheric anomaly before each earthquake; The blank space indicates that there were no TEC anomalies over the epicenter before the earthquake. The colors represent earthquake magnitudes, with blue (earthquakes 2, 4, 5, 6, and 7) representing magnitudes 6.5 to 6.7, green (earthquakes 9, 11, 12, and 13) representing magnitudes 6.8 to 6.9, and brown (earthquakes 14, 15, 16, and 20) representing magnitudes 7.0 to 7.3.The No. 9 earthquake has a maximum amplitude of 28.3, the No.7 earthquake has a maximum amplitude of 27.6, and the No. 4 earthquake has a maximum amplitude of 28.3, which indicates that the maximum amplitude of earthquakes between magnitudes 6.5 and 6.7 increases with magnitude except for the No. 4 earthquake. This phenomenon also exists for earthquakes between 6.7 and 6.9, and for subsequent earthquakes between 7.0 and 7.3, the maximum amplitude increases with magnitude, except for the No. 13 earthquake, which has a maximum amplitude of 55.3, which is higher than the No. 14 earthquake, which has a maximum amplitude of 49.4.

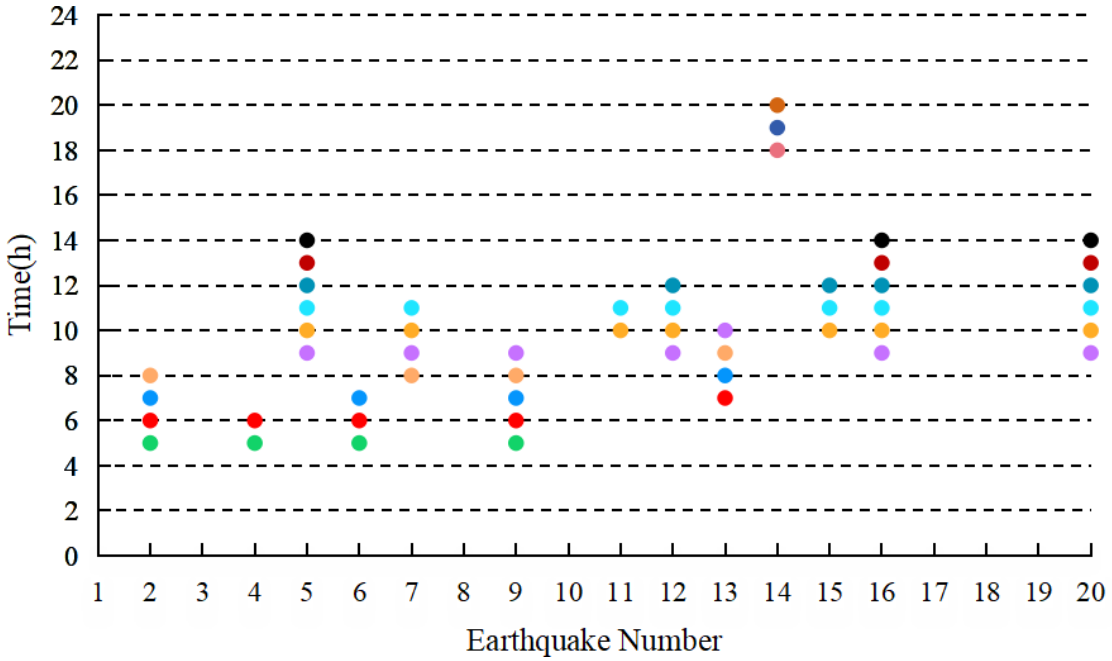


Figure 11 TEC anomaly occurrence time before each earthquake (UTC)

According to the above analysis method, the most obvious ionospheric anomaly before the earthquake was also used to analyze and make statistics on the occurrence time of each anomaly within one day (UTC). The results are shown in Figure 11. It can be seen from Figure 11 that, except for earthquake No. 14, other earthquake TEC anomalies all occurred after UTC5 and before UTC14, and it can also be observed that with the increase of earthquake magnitude, the occurrence time of earthquake may be delayed

**Case study**

In Figure 9, TEC anomaly was detected on the 29th day before the 20th earthquake (February 15, 2022) after excluding the influence of solar activity and geomagnetic activity. Since almost all anomalies in previous studies were observed 15 days before the earthquake, this special phenomenon will be analyzed in this paper. On March 16, 2022, a 7.3 magnitude earthquake occurred in Japan, the epicenter was located (141.58° E, 37.71° N), the focal depth of 41km, the TEC anomaly will be analyzed in detail below.

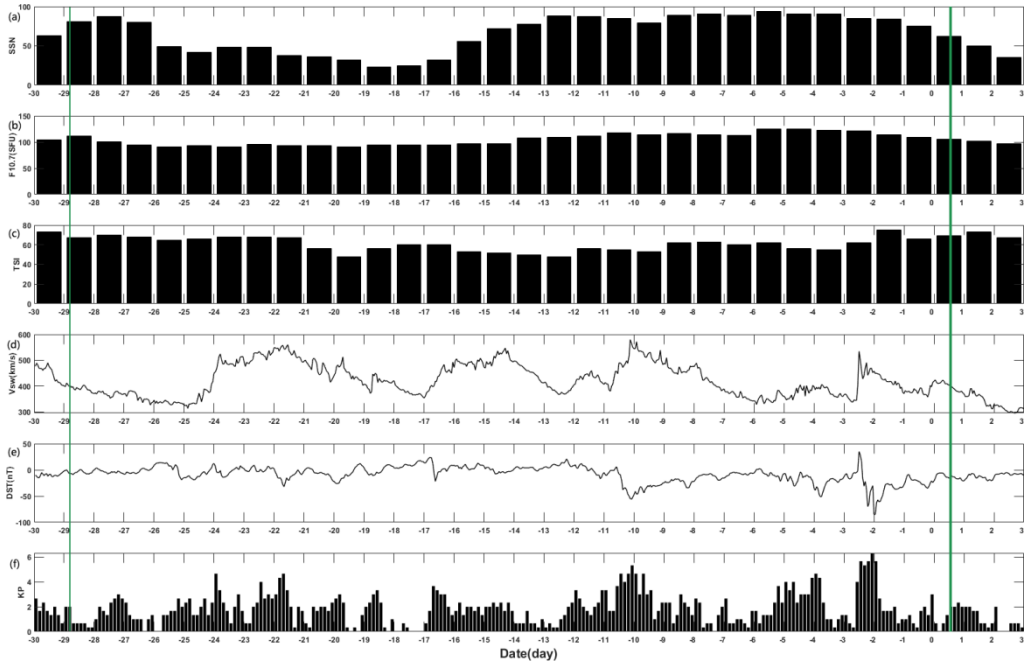


Figure 12. Solar and geomagnetic activity from 14 February to 18 March 2022 (UTC); The thick green line represents the time when the earthquake occurred, and the thin green line represents the time when the ionospheric anomaly occurred

Solar activity and geomagnetic storms have a great influence on ionospheric disturbances. Therefore, in order to eliminate these factors affecting ionospheric anomalies, six indices (SSN, F10.7, TSI, Vsw, Dst and KP) were used in this paper to estimate solar and geomagnetic activities. The solar-terrestrial environmental changes from 30 days before the earthquake to two days after the earthquake were shown in Figure 11. The thick green line represents the time when the earthquake occurred, and the thin green line represents the time when the ionospheric anomaly was detected. As shown in Figure 12(a)(b)(c)(d), the solar variation is relatively stable on February 15, 2022. The SSN index is about 70, the F10.7 index is about 100SFU, and the change of TSI and Vsw data is not obvious. Figure 12(e)(f) shows the DST and KP time series. The DST index measures changes in the storm ring current index, while the KP index measures geomagnetic activity on a global scale, and it is clear that the geomagnetic environment around February 15 was relatively calm in both data. Although there was a large degree of geomagnetic solar activity on 24, 10, and 2 days before the earthquake, there was no solar and geomagnetic activity anomaly on February 15 before the earthquake. We will continue to analyze the TEC anomaly changes on this day by using VTECmap.

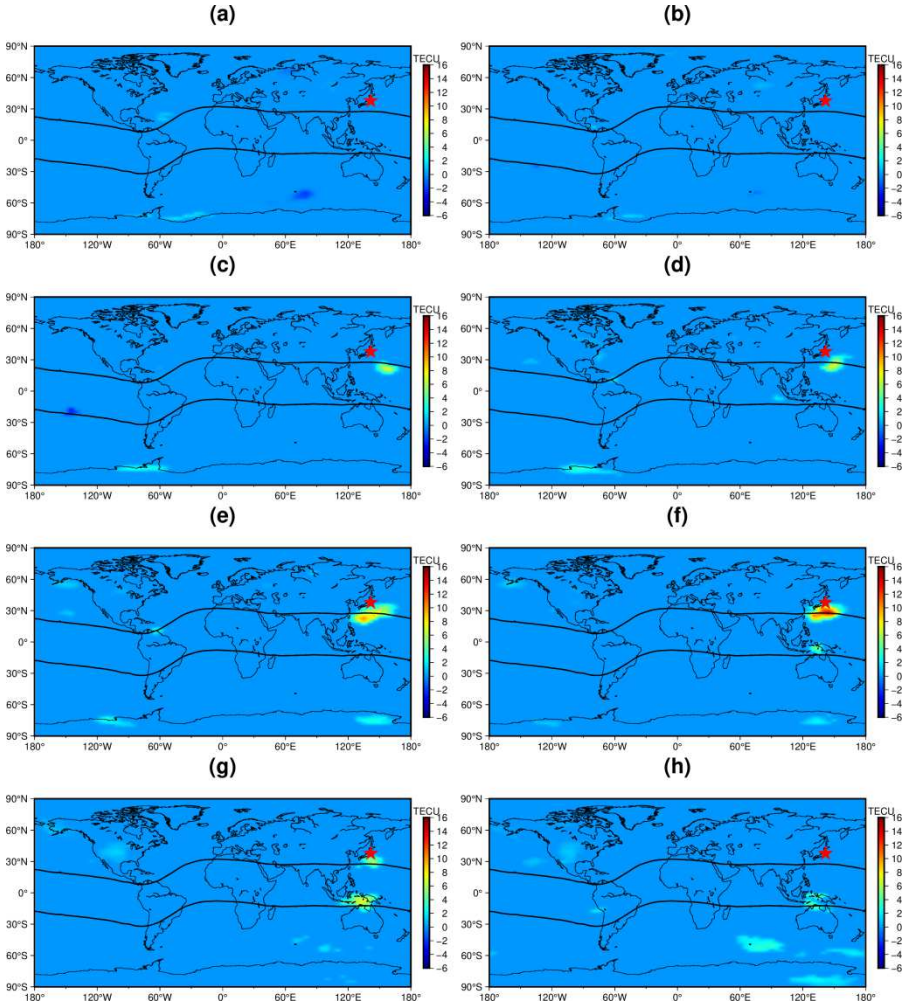


Figure 13. Global ionospheric changes from 00:00 to 7:00 on February 15, 2022; (a)UTC 00:00; (b)UTC 01:00; (c)UTC 02:00; (d) 03:00 UTC; (e) 04:00 UTC; (f) 05:00 UTC; (g) 06:00 UTC; (h) 07:00 UTC; The red five-pointed star represents the sky above the epicenter, and the black curve represents the magnetic equatorial line

Figure 13 shows the global TEC anomaly between UTC 00:00 and UTC 07:00 on February 15, 2022. From the figure, it can be seen that the global ionosphere was relatively quiet from UTC 00:00 to UTC 01:00, with an anomaly of amplitude of 6TECU southeast of the epicenter at UTC2. As time went by, the anomaly area gradually increased and moved westward to near the epicenter. The TEC anomaly amplitude reached a maximum of 14TECU at UTC5, and at the same time, corresponding TEC anomalies were also detected in the magnetic conjugate region, but the scale and amplitude were small. At UTC6, the TEC anomaly area in the magnetic conjugate region reaches the maximum, while the TEC anomaly area and

amplitude near the epicenter gradually decrease. At UTC 07:00, the TEC anomaly near the epicenter disappeared, and the TEC anomaly in the corresponding magnetic conjugate region gradually decreased until disappeared. During the period of TEC anomaly, TEC in other parts of the world did not show particularly obvious anomalies, and the amplitude was small. TEC anomalies caused in the space environment usually have different degrees of irregular ionospheric abnormal disturbance in a large geographical range, and only the seismic-ionospheric characteristics are shown in the changes of TEC anomalies. All kinds of phenomena indicate that such anomalies are not caused by solar or geomagnetic activities, but may be related to subsequent earthquakes.

The physical mechanism of the seismo-ionospheric effect has always been a key issue in the study of ionospheric abnormal disturbances before earthquakes. In many studies, the explanation of the physical mechanism of the seismo-ionospheric effect is mainly divided into three directions: the energy generated by earthquakes propagates to the Earth's surface in the form of seismic waves to stimulate atmospheric fluctuations. In particular, gravity waves have the most significant effect. These fluctuations propagate to the ionosphere and cause fluctuations in the ionosphere, which lead to changes in electron density, and then cause abnormal disturbances in the ionosphere. The change of ionospheric conductivity caused by radon and other carrier gases such as carbon dioxide, hydrogen, methane and helium escaping to the surface leads to the abnormal ionospheric electron concentration [28], which then produces the ionization effect of air and leads to the change of electron density [29]. And the Freund model of rock stress [30-31], which indicates that the rock under stress activates the forward hole electric load flow to generate current, resulting in the flow of electrons between the ground and the bottom of the ionosphere. This model has been verified to be reliable by experimental measurements [32]. However, the disadvantage of the Freuchian model is that it is not effective for earthquakes in the high seas, where ionospheric anomalies have been shown to occur at least as often as terrestrial earthquakes [33]. At present, the lithosphere-Atmosphere-ionospheric coupling model (LAIC) is widely used, and its action process is shown in Figure 14. According to the theory, the process observed in the ionospheric anomaly of large earthquakes is the air ionization phenomenon caused by the increase of the outflow of crustal gases (such as radon, helium, methane, carbon dioxide, etc.) near the active tectonic fault before the earthquake, which then triggers the reaction from the ground to the ionosphere and the magnetosphere, resulting in changes in the air conductivity and accompanied by rising temperature. Form temperature and pressure anomalies, outward wave infrared radiation (OLR) anomalies. This redistributes charge in the ionosphere [34], and local changes in ionospheric potential lead to irregular formation of electron and ion concentrations. In addition to the concentration of radon, atmospheric ionization is also affected by air temperature (temperature affects the movement speed of gas molecules and thus affects the probability of collision and ionization), air relative humidity (the concentration of water molecules determines the size of

newly formed ions), etc. [35]. Therefore, at high ionization level, large heavy ion clusters are easily formed at the atmospheric boundary above the seismogenic region before strong earthquakes, which will lead to higher ionization rate (with larger collision cross section), and then increase the electron concentration in the atmosphere, resulting in positive ionospheric anomalies. In addition, light ion aggregation will be formed in the atmosphere at the weak ionization level in the early stage of ionization. This results in a decrease in electron concentration at the boundary and a negative ionospheric anomaly. The ionization instability leads to the rise of ion temperature and the generation of acoustic gravity waves, which makes the plasma turbulence project along the high conductivity of the geomagnetic field to the magnetic conjugation region, resulting in the anomaly of the magnetic conjugation region.

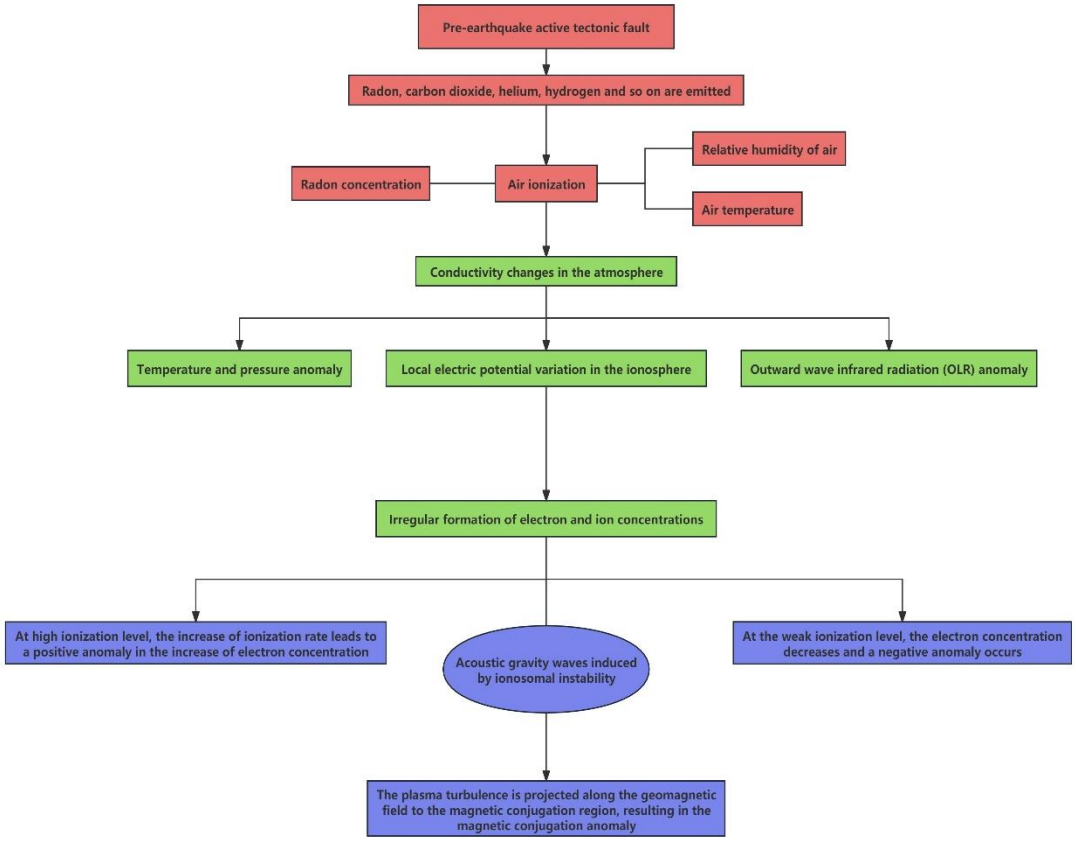


Figure 14. Action diagram of the lithosphere-Atmosphere-ionospheric coupling model (LAIC)

## 4. Conclusion

In this paper, the ionospheric anomalies of 20 Mw≥6.5 earthquakes occurred in Japan from 2011 to 2022 are studied and analyzed. The ionospheric anomalies affected by solar activities have a periodicity of 27 days by means of wavelet analysis. Subsequently, the solar and geomagnetic data of the selected earthquakes were processed by the sliding quartile distance method based on the 27-day window value, and the solar and geomagnetic activities were removed at the same time period as TEC anomalies to exclude the influence of solar and geomagnetic

activities on the ionosphere. All TEC outliers from 30 days before the earthquake to 2 days after the earthquake were obtained. Through the statistical analysis of the selected earthquakes, except for individual earthquakes, the overall TEC anomaly amplitude has a positive correlation with the magnitude to a certain extent, and the TEC anomaly duration tends to lag with the increase of the magnitude, but the relationship is not linear. Statistics show that 65% of earthquakes have TEC anomalies before the earthquake, and some earthquakes have multiple anomalies before the earthquake. It is worth noting that when analyzing the time of TEC anomaly, TEC anomaly disturbance was also found the 29th day before the 20th earthquake (February 15, 2022), which was inconsistent with previous studies. Through the analysis of solar and geomagnetic activities on that day, it was not significantly affected by solar activities at the time of TEC anomaly disturbance. Moreover, the geomagnetic environment is relatively calm on a global scale, so this disturbance is not due to solar or geomagnetic influence. VTECmap observed the global changes at the time when the anomaly occurred, but no obvious regular TEC anomalies appeared in other regions of the world at that time, and obvious seismic-ionospheric effects were observed over the epicenter, and TEC anomalies also appeared in the magnetic conjugate region corresponding to the epicenter. The subsequent analysis of the lithosphere-Atmosphere-ionospheric coupling model (LAIC) confirms that this phenomenon is a characteristic of the seismo-ionospheric coupling, thus proving that it is possible to detect pre-earthquake ionospheric anomalies 15 days before the earthquake.

**Author Contributions:** Z.L. and Z.T. designed the study and performed the experiments; Z.L. and Z.T. wrote the draft of the manuscript; L.H.C. supervised the research and revised the manuscript. All authors have read and agreed to the published version of the manuscript.

**Funding:** This work was financially supported by State Key Laboratory of Geo-Information Engineering (NO. SKLGIE2023-M-1-1) and Key Research Projects of Higher Education Institutions of Henan Provincial Education Department (NO. 24A420002)

**Data availability:** the sun and geomagnetic activity data taken by NASA's space physical facilities (SPDF) (https://spdf.gsfc.nasa.gov/index.html) and Belgian royal observatory Solar InfluencesData Analysis Provided by the Center: (https://www.sidc.be/); TEC data by The Center for Orbit Determinationin Europe (CODE) : (https://www.aiub.unibe.ch/services/index_eng.html)

**Acknowledgments:** We are very grateful to NASA's Space Physics Data Facility (SPDF) and the Solar Influences Data Analysis Center at the Royal Observatory of Belgium for providing solar and geomagnetic activity data. We thank The Center for Orbit Determinationin Europe (CODE) for providing the TEC data

**Conflicts of Interest:** The author declares no conflict of interest.

## References:


[1] Davies, K. & Baker, D. M. Ionospheric effects observed around the time of the Alaskan earthquake of March 28, 1964. *Journal of Geophysical Research*, *70*(9), 2251-2253 (1965).

[2] Zhao, B. et al. Is an unusual large enhancement of ionospheric electron density linked with the 2008 great wenchuan earthquake? *Journal of Geophysical Research Space Physics*. 113(A11) (2008).

[3] Li, J. et al. Ionospheric total electron content disturbance associated with May 12, 2008, Wenchuan earthquake. *J. Geodesy and Geodynamics*. 6(2): 126-134 (2015).

[4] Liu, J. Y. et al. Giant ionospheric disturbances excited by the M9.3 Sumatra earthquake of 26 December 2004. *J. Geophysical Research Letters*. 33(2): 356-360 (2006).

[5] Shah, M. & Jin, S. Pre-seismic ionospheric anomalies of the 2013 Mw=7.7 Pakistan earthquake from GPS and COSMIC observations. *J. Geodesy and Geodynamics*. 9(5): 378-387 (2018).

[6] Li, Z. et al. Analysis of Pre-Earthquake Space Electric Field Disturbance Observed by CSES. Atmosphere. *J. Atmosphere*. 13(6): 934 (2022).

[7] Xu, T. et al. Statistical analysis of seismo-ionospheric perturbation before 14 Ms≥7.0 strong earthquakes in Chinese subcontinent. *J. Chin J Radio Sci*. 27(3): 507-512 (2012).

[8] Dong, L., Zhang, X., & Du, X. Analysis of Ionospheric Perturbations Possibly Related to Yangbi Ms6. 4 and Maduo Ms7. 4 Earthquakes on 21 May 2021 in China Using GPS TEC and GIM TEC Data. *Atmosphere*. *13*(10), 1725 (2022).

[9] Freund, F. Pre-earthquake signals: Underlying physical processes. *Journal of Asian Earth Sciences*. 41(4-5), 383-400 (2011).

[10] Freund, F. Earthquake forewarning—A multidisciplinary challenge from the ground up to space. *J. Acta Geophysica*. 61, 775-807 (2013).

[11] Freund, F. Toward a unified solid state theory for pre-earthquake signals. *J. Acta Geophysica*. *58*, 719-766 (2010).

[12] Ouzounov, D. et al. Atmosphere-ionosphere response to the M 9 Tohoku earthquake revealed by multi-instrument space-borne and ground observations: Preliminary results. *Earthquake Science*. 24, 557-564 (2011).

[13] Ouzounov, D. et al. Transient effects in atmosphere and ionosphere preceding the 2015 M7. 8 and M7. 3 Gorkha–Nepal earthquakes. *Frontiers in Earth Science*. 9: 757358 (2021).

[14] Pulinets, S. A. Physical mechanism of the vertical electric field generation over active tectonic faults. *Advances in Space Research*. 44(6), 767-773 (2009).

[15] Pulinets, S. & Khachikyan, G. The Global electric circuit and global seismicity. *Geosciences*. 11(12), 491 (2021).

[16] Parrot, M. et al. Atmospheric and ionospheric coupling phenomena associated with large earthquakes. *The European Physical Journal Special Topics*. 230, 197-225 (2021).

[17] Thomas, E. G., Baker, J. B. H., Ruohoniemi, J. M., Coster, A. J., & Zhang, S. R. The geomagnetic storm time response of GPS total electron content in the North American sector. *Journal of Geophysical Research: Space Physics*. 121(2), 1744-1759 (2016).

[18] Afraimovich, E. L., Astafyeva, E. I., Oinats, A. V., Yasukevich, Y. V., & Zhivetiev, I. V.

Global electron content: a new conception to track solar activity. *Annales Geophysicae. Göttingen, Germany: Copernicus Publications*. 26(2): 335-344 (2008).
[19] Liu, J. Y. et al. Seismoionospheric GPS total electron content anomalies observed before the 12 May 2008 Mw7. 9 Wenchuan earthquake. *Journal of Geophysical Research: Space Physics*. 114(A4) (2009).
[20] Chen, H., Han, P. & Hattori, K. Recent advances and challenges in the seismo-electromagnetic study: A brief review. *J. Remote Sensing*. 14(22): 5893 (2022).
[21] Guo, Y. et al. Seismo-Ionospheric Effects Prior to Two Earthquakes in Taiwan Detected by the China Seismo-Electromagnetic Satellite. *J. Atmosphere*. 13(9): 1523 (2022).
[22] Zhu, F., Zhou, Y., Lin, J., & Su, F. A statistical study on the temporal distribution of ionospheric TEC anomalies prior to M7. 0+ earthquakes during 2003–2012. *Astrophysics and Space Science*. 350, 449-457 (2014).
[23] Zhu, F., Wu, Y., Zhou, Y., & Gao, Y. Temporal and spatial distribution of GPS-TEC anomalies prior to the strong earthquakes. *Astrophysics and Space Science*. 345, 239-246 (2013).
[24] Collado-Villaverde, A., Muñoz, P. & Cid, C. Classifying and bounding geomagnetic storms based on the SYM-H and ASY-H indices. *J. Natural Hazards*. 2023: 1-22 (2023).
[25] Li, W., Guo, J., Yu, X., Yu, H. & Chang, X. Analysis of spatiotemporal variations in the ionosphere detected by gps. *Journal of Surveying and Mapping*. 031(006), 561-565,569 (2014).
[26] Shama, A. Spectrum compatible earthquake ground motions by morlet wavelet. In *20th analysis and computation specialty conference*. 2012: 163-172 (2012).
[27] Rapoport, Y. et al. Change of ionospheric plasma parameters under the influence of electric field which has lithospheric origin and due to radon emanation. *J. Physics and Chemistry of the Earth, Parts A/B/C*. 29(4-9): 579-587 (2004).
[28] Surkov, V. V. & Pilipenko, V. A. Estimate of ULF electromagnetic noise caused by a fluid flow during seismic or volcano activity. J. Natural Hazards and Earth System Sciences Discussions. 2(10): 6475-6497 (2014).
[29] Scoville, J. et al. Paradox of Peroxy Defects and Positive Holes in Rocks Part II: Outflow of Electric Currents from Stressed Rocks. *Journal of Asian Earth Sciences*. 114: 338-351 (2015).
[30] Roger, F., Jolivet, M. & Malavieille, J. The tectonic evolution of the Songpan-Garzê (North Tibet) and adjacent areas from Proterozoic to Present: A synthesis. *J. Journal of Asian Earth Sciences*. 39(4): 254-269 (2010).
[31] Liu, J. Y. & Chi-Kuang, C. An observing system simulation experiment for FORMOSAT-5/AIP detecting seismo-ionospheric precursors. *TAO: Terrestrial, Atmospheric and Oceanic Sciences*. 28(2): 1 (2017).
[32] Parrot, Michel. et al. Atmospheric and Ionospheric Coupling Phenomena Associated with Large Earthquakes. *The European Physical Journal Special Topics.* 230. 197-225 (2021).
[33] Harrison, R. G., Aplin, K. L. & Rycroft, M. J. Atmospheric electricity coupling between earthquake regions and the ionosphere. *J. Journal of Atmospheric and Solar-Terrestrial Physics*. 72(5-6): 376-381 (2010).
[34] Pulinets, S. Low-latitude atmosphere-ionosphere effects initiated by strong earthquakes preparation process. *J. International Journal of Geophysics*. 2012: 1-14 (2012).